THE JOURNAL OF PHYSICAL CHEMISTRY C

Article

pubs.acs.org/JPCC

Effect of the Al Siting on the Structure of Co(II) and Cu(II) Cationic Sites in Ferrierite. A Periodic DFT Molecular Dynamics and FTIR Study

Stepan Sklenak,*[†] Prokopis C. Andrikopoulos,[†] Sarah R. Whittleton,[†] Hana Jirglova,[†] Petr Sazama,[†] Lubomir Benco,[‡,∥] Tomas Bucko,[‡,§,∥] Juergen Hafner,[‡] and Zdenek Sobalik[†]

[†]J. Heyrovský Institute of Physical Chemistry of the Academy of Sciences of the Czech Republic, Dolejškova 3, 182 23 Prague 8, Czech Republic

[‡]Institut für Materialphysik and Center for Computational Materials Science, Universität Wien, Sensengasse 8, A−1090 Vienna, Austria

[§]Department of Physical and Theoretical Chemistry, Faculty of Natural Sciences, Comenius University, Mlynska Dolina, SK-84215 Bratislava, Slovakia

[∥]Institute of Inorganic Chemistry, Slovak Academy of Sciences, Dubravska cesta 9, SK-84236 Bratislava, Slovakia

Supporting Information

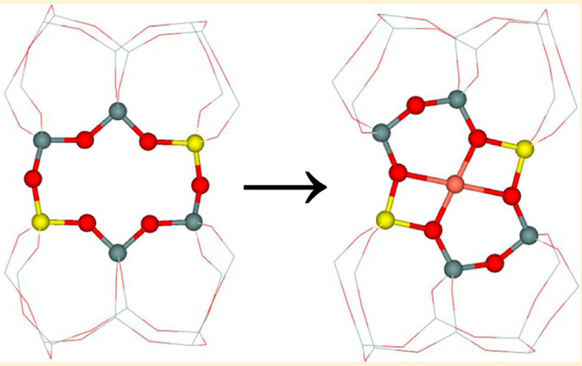

ABSTRACT: Periodic DFT molecular dynamics and FTIR spectroscopy were used to investigate the cationic sites of ferrierite exchanged with Co(II) and Cu(II) and their complexes with NO. Particular attention was paid to the effect of the Al siting in six-membered rings forming the cationic sites on the structure of these sites and the corresponding binding energies of Me(II) (Me = Co and Cu). Our calculations show that both the cations upon binding to cationic sites induce a rearrangement of the local structure of the zeolite framework. The rearrangement is significant for the α and β-2 sites while it is minor for the β-1 site. Comparison of the observed and theoretical NO stretching frequencies of ferrierite Co(II) and Cu(II) complexes with a NO molecule permitted the assignment of IR bands to the individual types of cationic sites. For NO-Co-ferrierite, the IR bands found at 1956, 1941, and 1935 cm^{-1} can be assigned to NO-Co complexes with Co(II) located in the α, β-1, and β-2 sites, respectively. Similarly for NO-Cu-ferrierite, the frequencies of 1864, 1912, 1904, and 1892 cm^{-1} belong to NO-Cu complexes having Cu(II) accommodated in the α, β-1, β-2 (conformer 1), and β-2 (conformer 2) sites, respectively. The calculated adsorption energies are systematically higher for Co(II) than for Cu(II) for all the three sites and are in the order $\alpha > \beta\text{-2} > \beta\text{-1}$ for both the cations. Our computational results further reveal that upon binding Me(II) both the local structure of the zeolite framework as well as the binding energies of Me(II) strongly depend on the Al siting in the rings forming the cationic sites. The calculated relative binding energies of Me(II) are in the order $\beta\text{-1} > \beta\text{-2} > \alpha$ for both the cations. The general tendency of Me(II) accommodated in a cationic site to react is inversely proportional to the corresponding binding energies. We also showed that FTIR spectroscopy of complexes of NO and Me(II)-exchanged ferrierite can serve to identify the Al siting in the six-membered rings forming cationic sites.

1. INTRODUCTION

Silicon-rich zeolites (Si/Al > 8), such as ZSM-5, mordenite, ferrierite, and beta zeolites, represent catalytic materials with wide industrial application. Their transition-metal-exchanged forms were discovered as exceptional redox catalysts.[1,2] Cu-zeolites[3−5] together with Fe-zeolites[6−8] are the two most important systems as they have real potential for application in deN_2O and deNO_x processes under real conditions. Cu-zeolites were studied as catalysts for a spectrum of related environmental processes, such as N_2O decomposition and N_2O selective catalytic reduction (SCR), for direct NO decomposition as well as for SCR of NO_x using various reducing agents.[9] Co-zeolites are currently the most viable catalysts for effectively reducing NO_x by methane without producing N_2O or CO byproducts in oxygen-rich streams.[10−16] Besides methane, propane can be used as a reducing agent in the Co-zeolite-catalyzed C_3H_8-SCR-NO_x process.[17]

Knowledge of the structure of active sites accommodating transition-metal cations in frameworks of silicon-rich zeolites is of crucial importance to understand the catalytic activity of these catalysts. Diffraction methods are of limited use in determining the structure of the cationic sites of divalent cations in frameworks of silicon-rich zeolites. The structures of sites binding divalent cations were estimated using X-ray

Received: October 16, 2012
Revised: January 5, 2013
Published: January 7, 2013

dx.doi.org/10.1021/jp310236d | J. Phys. Chem. C 2013, 117, 3958−3968

diffraction experiments only for mordenite[18−20] and ferrierite frameworks.[21−24] However, the obtained structures of the cationic positions represent a superposition of different arrangements of these sites with and without accommodated divalent cations. Moreover, some rings forming vacant cationic sites contain two Al atoms which are needed for the site to bind a divalent cation, while other rings include only one or no Al atom (rings that are not able to accommodate a bare divalent cation). These issues result in a significant decrease in the accuracy of the X-ray diffraction-determined structure of the framework oxygen atoms involved in coordinating the divalent cation. However, the structure of sites accommodating a divalent cation can be inferred from theoretical calculations.[25]

Traditionally, zeolites were modeled using cluster and later embedded-cluster modeling approaches. Here, a finite, usually rather small environment of the active sites is described using mainly DFT,[26] and if an embedded-cluster method (or QM/MM) is employed, then the cluster is embedded in a larger structure (nonperiodic calculations) or a supercell (periodic computations) of the zeolite framework. These approaches have been used to investigate the structure and properties of sites binding divalent cations in frameworks of zeolites.[26−30] Periodic DFT methods which allow calculations of full unit cells or supercells composed of several unit cells are now routinely available,[26] but spin-polarized periodic DFT methods which permit computations of transition-metal-exchanged silicon-rich zeolites became feasible a few years ago.[26] For example, Sklenak et al. investigated Fe-ferrierite,[25] Li et al. computed Fe-ZSM-5,[31] Benco et al. calculated Zn-mordenite,[32] and Göltl and Hafner studied Co-chabazite and Cu-chabazite.[33,34]

Nitric oxide is a frequently used FTIR probe of the oxidation state and the local coordination environment of transition-metal cations accommodated in zeolite frameworks. There have been several periodic DFT studies of complexes of NO molecules with transition-metal-exchanged zeolites. Benco et al. investigated NO-Fe-ferrierite,[35,36] Georgieva et al. studied NO-Co-chabazite, NO-Co-mordenite, and NO-Co-ferrierite,[37] Grybos et al. calculated NO-Pd-mordenite,[38] and Göltl and Hafner computed NO-Co-chabazite and NO-Cu-chabazite.[39]

In agreement with experimental evidence, all these calculations accepted the model of a bare cation located in an extraframework position of a zeolite. This model is consistent with the experimental data showing divalent transition metal cations balancing the negative charge of two Al atoms located in a cationic site created by a six-membered ring[40] in the framework of a silicon-rich zeolite. The location of a divalent bare cation in the vicinity of only one framework Al with a distant second framework Al is of very low probability because of the high reactivity of such a cation.[35] Since Al-O-Si-O-Al sequences in frameworks of zeolites with Si/Al > 8 are not present,[41,42] cationic sites are formed by Al-O-Si-O-Si-O-Al sequences located in six-membered rings creating the cationic sites. There are more possible nonequivalent arrangements of Al-O-Si-O-Si-O-Al in the rings (hereafter called Al siting in the rings) depending on the type of the site and the zeolite framework. An obvious question is whether various Al sitings in the rings can influence the structure of the cationic sites and the binding energies of the accommodated cations and thus also affect their properties as potentially catalytically active sites.

It is difficult to differentiate in experiments the activity of such individual active sites in the zeolite catalyst with various Al sitings in the rings forming these active sites. Conversely, theoretical modeling allows the evaluation of the effect of the Al siting in the rings forming cationic sites on the potential reactivity of the catalytically active species. For example, our periodic DFT study of the N_2O decomposition over Fe-ferrierite revealed a significantly different reactivity of the iron cation accommodated in the sites with different Al sitings in the rings forming the cationic sites.[25,43]

In this article, we use periodic DFT and FTIR spectroscopy to investigate the cationic sites of ferrierite exchanged with Co(II) and Cu(II), which are typical representatives of transition metals used in zeolite-based catalysts. We examine the changes of the local structure of the zeolite framework upon accommodation of Me(II) (Me = Co and Cu) cations and upon formation of complexes of NO with Me(II). Further, we study the binding energies of Me(II) in these cationic sites and thus their general tendencies to react. The NO molecule, which is an important and versatile probe of cationic sites as well as a reactant in the deNOx types of reactions, is employed to reveal the local coordination environment of the Me(II) cations located in the active sites and to validate the calculated results. For these purposes, FTIR spectroscopy of metal−cation complexes with a NO molecule is used, and experimental results are compared with those calculated by the periodic DFT approach. We also study the effect of the Al siting in six-membered rings forming the cationic sites on the structure of these sites and the corresponding binding energies of Me(II). In addition, we explore the possible determination of the Al siting in the six-membered rings of ferrierite forming cationic sites using FTIR spectroscopy of metal−cation complexes of ferrierite with a NO molecule.

2. EXPERIMENTAL SECTION

2.1. Ferrierite Samples. Ferrierite (Tosoh, Japan; Si/Al 8.6) was used. The sample was the same as that used in our prior studies.[8,25,44,45] The parent zeolite was transformed by a repeated ion-exchange with NH_4NO_3 into the NH_4-form.

Co-ferrierite and Cu-ferrierite samples were prepared as follows: the NH_4-form of the parent zeolite was repeatedly ion-exchanged using 0.1 and 0.05 M solutions of $Co(NO_3)_2$ and $Cu(NO_3)_2$, respectively, washed out by distilled water, and then filtrated and dried at low temperature (~105 °C). The Co/Al and Cu/Al ratios were determined by chemical analysis of the prepared samples to be 0.12 and 0.09, respectively. Both the values are significantly below the maximum ion-exchange capacity for Me(II) cations, which is 0.33 for the parent used.[44] Nevertheless, both the β as well as α sites are partially occupied by Co(II) and Cu(II) at these Me(II)/Al values.[46,47]

2.2. FTIR Spectroscopy. FTIR spectra of the Co-ferrierite and Cu-ferrierite samples were measured at room temperature with a resolution of 2 cm^{-1} using a Magna 550 (Thermo Nicolet) spectrometer. The samples were used as self-supported pellets with the thickness from 5 to 10 mg/cm^2. The spectra intensities were normalized on the sample with the thickness of 5.5 mg/cm^2 using the integral area of the zeolite skeletal bands in the region between 1750 and 2100 cm^{-1}. The samples were simultaneously dehydrated (at 450 °C) and evacuated (10^{-3} Pa) in a glass vacuum cell equipped with six position carousel holder and NaCl windows before they were dosed with NO at room temperature. FTIR spectra were measured after 30 min of adsorption of NO. Our goal was to prepare mononitrosyl complexes of both Cu-ferrierite and Co-ferrierite. Therefore, in the case of Co-ferrierite, the adsorption was followed by an evacuation at elevated temperature (~200

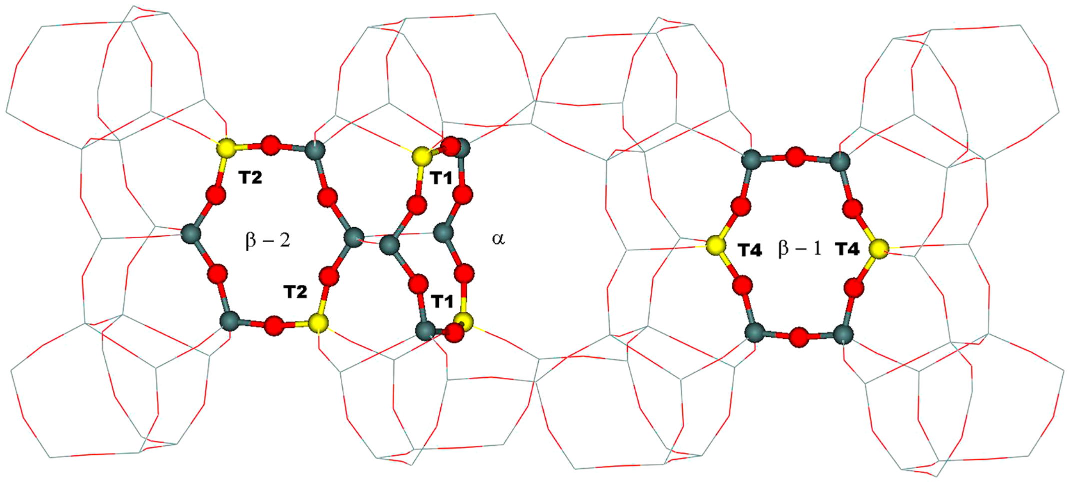

Figure 1. Structure of the *α*, *β*-1, and *β*-2 sites. Silicon atoms are in gray, oxygen atoms in red, and aluminum atoms in yellow.

°C). The band positions were identified by a Fourier self-deconvolution procedure (OMNIC 4.1 software). Final data processing was carried out using the OriginPro 7.5 software (MicroLab Corporation).

3. CATIONIC SITES IN FERRIERITES

3.1. Type and Structure of Cationic Sites. Bare divalent metal cations can occupy three types of cationic sites in ferrierites designated as *α*, *β*, and *γ*. They were first suggested by employing UV−vis spectroscopy of bare Co(II) ions as a probe[48] and later confirmed by synchrotron powered XRD.[21−24] The *α*, *β*, and *γ* sites are also reflected in FTIR spectra of Me(II)-exchanged ferrierites.[49]

Figure 1 shows the structure of the *α* and *β* sites while the *γ* site is not depicted since the concentration of framework Al atoms forming the *γ* site in ferrierites is very low, and therefore this site is not considered in this study. The *α* cationic site represents an elongated six-membered ring which is composed of two five-membered rings. This site is easily accessible because it is present on the wall of the main channel in ferrierite. The *β* cationic site in ferrierite corresponds to a deformed six-membered ring. This site can be easily reached because it is positioned in an eight-membered ring channel of ferrierite.

As shown previously, there is a general preference for the occupation of the *β* site during an ion-exchange of divalent cations while the *α* site is occupied by Me(II) to a lower extent. Therefore, the *α* site represents a minority component in comparison with the occupation of the *β* site in samples with a medium level of exchange.[46,47,50]

3.2. Al Siting in the Rings Forming Cationic Sites. Two Al atoms located in six-membered rings creating cationic sites can exhibit more possible nonequivalent Al sitings in the rings forming these cationic sites, i.e., two Al atoms occupy different pairs of distinguishable T sites (Figure 1). It has been shown that the Al siting[50−52] (i.e., which different distinguishable framework T sites are occupied by isolated Al atoms[50]) and the Al distribution[47,50,53−57] (i.e., distribution of the framework Al atoms between Al-O-Si-O-Si-O-Al sequences in the rings forming cationic sites for divalent cations and isolated Al atoms[50]) can significantly affect the catalytic activity of catalysts based on silicon-rich zeolites. Similarly, we assume that in analogy to the above-mentioned effects variation in the Al siting in the rings forming cationic sites can potentially influence the catalytic activity of the accommodated metal cations.

Before possible effects of the Al siting in the rings can be experimentally studied, it is necessary to identify the types of cationic sites and the Al siting in the rings of these cationic sites in the investigated material. There is only one direct method, to the best of our knowledge, which permits this identification in ferrierite. This method is ^{27}Al MQ MAS NMR spectroscopy combined with DFT calculations.[44] Conversely, analysis of Mössbauer spectra of ^{57}Fe-ferrierite[45,58] can likely yield the occupations by Fe(II) of the cationic sites with the various Al sitings in the ring.

Several studies have shown that the Al distribution in the zeolite framework depends on the conditions of zeolite synthesis.[44,59−62] Therefore, we assume that the Al siting in the rings forming cationic sites can differ in samples of the same type of zeolite (even with the same Si/Al ratio) which were prepared under various conditions of their synthesis. Therefore, one of the goals of this study is a development of another method which allows an identification of the Al siting in the rings forming cationic sites. For this purpose we employ FTIR spectroscopy of metal−cation complexes of ferrierite with a NO molecule along with DFT calculations.

Our previous ^{29}Si MAS NMR experiments revealed that Al-O-Si-O-Al sequences are not present in the ferrierite sample used,[25,44] and therefore, the two Al atoms form Al-O-Si-O-Si-O-Al sequences in the six-membered rings.[41,42,63] Thus, there is only one possible Al siting in the rings in the *α* site while there are two possible Al sitings in the rings forming the *β* sites which are designated as the *β*-1 and *β*-2 sites (Figure 1).[25,35,36,44,45]

3.3. Cationic Sites in the Ferrierite Sample Used. The parent sample (ferrierite, Tosoh, Japan; Si/Al 8.6) was thoroughly investigated in our previous studies by UV−vis spectroscopy,[44] ^{27}Al 3Q MAS NMR spectroscopy,[44] FTIR spectroscopy,[45] and Mössbauer spectroscopy.[45]

Analysis of the visible spectra of the maximum Co(II)-exchanged ferrierite sample reveals that Al-O-Si-O-Si-O-Al sequences are predominantly located in the six-membered rings of the *β* cationic site (50% of all the framework Al atoms) while the rest of the sequences are present in the *α* site (10% of all the framework Al atoms).[44] The remaining 40% of Al in the zeolite framework are isolated Al atoms.[44] UV−vis spectroscopy of the maximum Co(II)-exchanged sample cannot distinguish between the *β*-1 and *β*-2 sites.[64,65] Our ^{27}Al 3Q

MAS NMR spectroscopy study identifies the presence of the β-2 and α sites in the ferrierite used.[44] On the other hand, our investigation of ^{57}Fe-ferrierite employing FTIR and Mössbauer spectroscopies allows a tentative assignment of the Mössbauer parameters to Fe accommodated in the α, β-1, and β-2 sites. If the tentative assignment of the Mössbauer parameters holds then both the β-1 and β-2 sites are present in the ferrierite framework, however, the concentration of Al-O-Si-O-Si-O-Al sequences creating β-1 is about an order of magnitude smaller (~3% of all the framework Al atoms) than that corresponding to β-2 (~47% of all the framework Al atoms).[45] This most likely explains why ^{27}Al 3Q MAS NMR spectroscopy showed only the β-2 sites as the concentration of the sites with the β-1 arrangement was beyond the detection limit of the method.[44]

4. COMPUTATIONAL DETAILS

4.1. Structural Models. Three models, designated as the α, β-1, and β-2 models, possessing the $P1$ symmetry, were employed. They feature one unit cell of ferrierite with two Al/Si substitutions forming the respective α, β-1, and β-2 cationic sites, accommodating Co(II) and Cu(II) cations. Two sets of calculations were carried out. The first featured bare cations in the zeolite (Co-ferrierite and Cu-ferrierite) while the other also included one NO molecule adsorbed by the N atom on the Co(II) and Cu(II) cations (NO-Co-ferrierite and NO-Cu-ferrierite, respectively). The coordination of NO by the O atom on Me(II) is much weaker[35] and is not considered in this study. In addition, the investigation of Co(II) complexes with multiple NO ligands is beyond the scope of this study. The starting structure of the all-silica framework was generated from the experimental orthorhombic structure of ferrierite determined by neutron diffraction.[66]

4.2. Electronic Structure Calculations. Periodic DFT calculations were carried out employing the VASP code.[67−70] The high-spin electron configuration Co $d^5\uparrow d^2\downarrow$ and the electron configuration Cu $d^5\uparrow d^4\downarrow$ were employed for the Co(II) and Cu(II) cations, respectively, accommodated in the zeolite. The adsorption of NO leads to the pairing of the NO $\pi^*\downarrow$ electron with an unpaired Co and Cu d electron and to a decrease of the magnetic moment to 2 μB for the Co(II)-NO cluster and to a formation of a nonmagnetic configuration for the Cu(II)-NO cluster in the zeolite. The Kohn−Sham equations were solved variationally in a plane-wave basis set using the projector-augmented wave (PAW) method of Blöchl,[71] as adapted by Kresse and Joubert.[72] The exchange-correlation energy was described by the PW91 generalized gradient approximation (GGA) functional.[73,74] Brillouin zone sampling was restricted to the Γ-point. The plane-wave cutoff of 400 eV was utilized for geometry optimizations while a smaller cutoff of 300 eV was used for the molecular dynamics simulations.

4.3. Geometry Optimizations. The atomic positions were optimized at constant volume employing a conjugate-gradient algorithm minimization of energies and forces while the lattice parameters were fixed at their experimental values.

4.4. Molecular Dynamics. The molecular dynamics (MD) simulations used the exact Hellmann−Feynman forces acting on atoms and applied the statistics of the canonical ensemble to the motion of the atomic nuclei[75] using the Verlet velocity algorithm[76,77] to integrate Newton's equations of motion. The time step for the integration of the equations of motion was 1 fs. The simulations were run for 5 ps at 300 K. The structures of ten distinct "snapshots" collected from the last 500 fs of each molecular dynamics simulation were optimized. Harmonic vibrational frequencies were calculated for the optimized conformers of the Co(II)- and Cu(II)-exchanged ferrierites forming a complex with one NO molecule (NO-Co-ferrierite and NO-Cu-ferrierite).

4.5. Vibrational Frequencies. Harmonic vibrational frequencies of the calculated systems were calculated using the finite differences method.[78] No atoms were kept frozen.

4.6. NO Adsorption Energies. The adsorption energy ΔE_{ads} of NO on Me-ferrierite was calculated as the difference between the energy of NO-Me-ferrierite and the sum of energies of Me-ferrierite and NO. NO was optimized in the empty unit cell with the same cell parameters as Me-ferrierite. ΔE_{ads} was calculated for NO-Me-ferrierite structures optimized both before and after the MD calculations.

4.7. Relative Binding Energies of Co(II) and Cu(II) in Co-Ferrierite and Cu-Ferrierite, Respectively. The absolute values of the binding energies ($\mathrm{BE_{Me}}$) of Me(II) cannot be computed accurately due to difficulties to calculate isolated Me(II) using periodic DFT; therefore, we evaluated the relative binding energies ($\Delta\mathrm{BE_{Me}}$)[79] using the difference between the energies of the Me-ferrierite featuring the site of interest and the Me-ferrierite with the most stable site (β-1 in all cases). This energy gap was corrected by subtracting the difference between the energies of the ferrierite with the empty site of interest and the ferrierite featuring the most stable site without the cation. The empty sites have two Al atoms in the corresponding six-membered ring forming the cationic sites which are not compensated by any cation.

$$\begin{aligned}\Delta\mathrm{BE_{Me}} &= E_{\text{site of interest}} - E_{\text{most stable site}}\\ &\quad - (E_{\text{empty site of interest}} - E_{\text{empty most stable site}})\end{aligned}$$

5. EXPERIMENTAL RESULTS

The FTIR spectra of Co-ferrierite and Cu-ferrierite exposed to NO (Figure 2) show the presence of the bands corresponding to mononitrosyl and polynitrosyl species in the 2000−1750 cm^{-1} region. The species are mainly dinitrosyl complexes

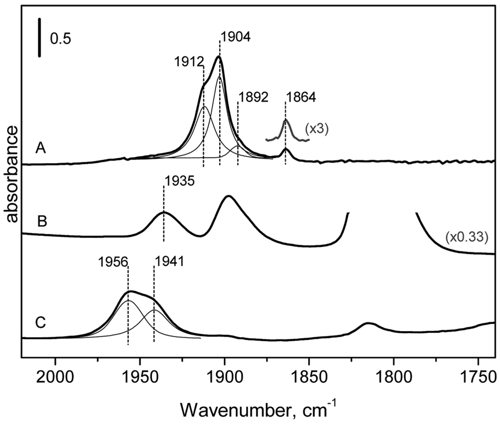

Figure 2. FTIR spectra of Co-ferrierite and Cu-ferrierite after adsorption of NO at room temperature. Spectra of Cu-ferrierite (Cu/Al 0.09) after adsorption of 38 Torr of NO (A) and of the Co-ferrierite (Co/Al 0.12) after adsorption of 10 Torr of NO (B) and after the subsequent evacuation of the Co-ferrierite at 200 °C for 30 min (C). The spectra of the zeolite prior to NO adsorption and the gas phase are subtracted. The thin lines represent bands components obtained by fitting the measured spectra by the Voigt function.

formed on Co-ferrierite sample (bands in the 1920−1750 cm^{-1} region) and mononitrosyl complexes over Cu(II) cations (bands from 1920 to 1850 cm^{-1}). Under the experimental conditions there were observed only negligible intensities of Cu(I) mononitrosyl and dinitrosyl species (i.e., IR bands expected in the region below 1845 cm^{-1}), indicating that most of the copper cations are in the Cu(II) state at the moment of the NO introduction.[80,81] This observation can be explained by a high content of sites binding divalent cations in the ferrierite used[44] and a preference of Cu(II) to exchange into such sites at a low Cu/Al ratio.[46] It is well-known that Co(II) has a high tendency to form dinitrosyl species,[46,80,81] and thus the structure of the IR bands of the mononitrosyl species over Co-ferrierite was apparent only after a desorption at elevated temperatures (~200 °C) due to a substantial reduction of the intensity of the pair of dinitrosyl bands at around 1890 and 1820 cm^{-1}.

The positions of the IR bands of mononitrosyl complexes formed on Cu(II) of Cu-ferrierite are observed at 1912, 1904, 1892, and 1864 cm^{-1}, while the IR bands at 1956, 1941, and 1935 cm^{-1} belong to the mononitrosyl species of Co(II) of Co-ferrierite.

It should be stressed that the intensities of the IR bands do not simply correspond to the amount of the corresponding species (i.e., Me(II) accommodated in a particular site) in the zeolite. Nevertheless, our goal was the identification of the positions of the individual mononitrosyl IR bands corresponding to NO interactions with Co(II) and Cu(II) cations in the cationic sites of ferrierite as a base for a validation of the calculated results and, more importantly, a determination of the Al siting in the rings forming the active sites.

6. COMPUTATIONAL RESULTS

6.1. Structure and Stability of the Co(II) and Cu(II) Cationic Sites.

Our calculations of the three models (*α*, *β*-1, and *β*-2) of Co-ferrierite, NO-Co-ferrierite, Cu-ferrierite, and NO-Cu-ferrierite yielded the structures and stabilization energies (Table 1) of the *α*, *β*-1, and *β*-2 sites for both the cations. There are two distinct conformers computed for the *β*-2 model of NO-Cu-ferrierite which have essentially the same energies. They differ mainly in the length of one of the Cu-O bonds (2.697 and 2.836 Å). All the other distinct conformers of all the calculated systems are higher in energy by at least 5 kcal/mol, and they are not considered in this study.

Table 1. Stabilization Energies[a] in kcal/mol of the Cationic Sites Accommodating Co and Cu

	cationic sites		
	α	*β*-1	*β*-2
Co-ferrierite	6.0	1.4	9.6
Cu-ferrierite	10.9	2.1	12.0
NO-Co-ferrierite	2.5	1.6	9.6
NO-Cu-ferrierite	5.6	3.6	11.9, 11.8[b]

[a] The difference between the energies of the model relaxed by MD simulations and subsequently optimized and the model which was not relaxed by MD simulations but simply optimized using the starting structure determined by neutron diffraction.[66] [b] The two values correspond to two distinct conformers.

6.1.1. Co-Ferrierite and Cu-Ferrierite. The optimized structures before and after the MD calculations are shown in Figures 3−5 and Figures S1−S6 of the Supporting Information.

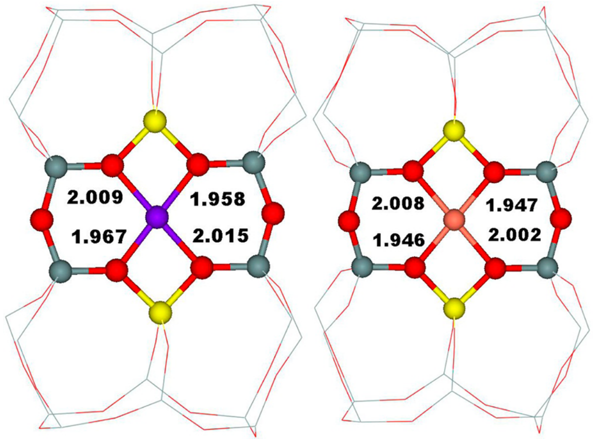

Figure 3. Optimized structures of the *β*-1 site of Co-ferrierite (left) and Cu-ferrierite (right) after molecular dynamics simulations. The distances are in angstroms. Silicon atoms are in gray, oxygen atoms in red, aluminum atoms in yellow, cobalt atom in violet, and copper atom in pink.

The structure of the *β*-1 cationic site (Figure 3 and Figures S1 and S2) is only slightly changed, while the geometries of the *α* (Figure 4 and Figures S3 and S4) and *β*-2 (Figure 5 and Figures S5 and S6) cationic sites differ significantly after the MD simulations. The Co-O and Cu-O bond lengths in Co-ferrierite and Cu-ferrierite, respectively, optimized after the MD simulations range from 1.885 to 2.170 Å and 1.887 to 2.224 Å, respectively. Two Me-O bonds are shorter than the other two. The calculated Co-O bond lengths are in good agreement with those obtained by EXAFS measurements, which revealed two Co-O distances of 1.99 and 2.09 Å for Co-ferrierite with Co(II) located mainly in the *β* sites.[46] Our MD simulations of Me-ferrierites and subsequent optimizations of the selected MD snapshots led to energy stabilizations (Table 1) relative to the corresponding structures which were not relaxed by employing MD simulations but that were simply optimized using the structure determined by neutron diffraction[66] as the starting geometry. The stabilization energy (Table 1) is significant for the *α* (6.0 and 10.9 kcal/mol for Co-ferrierite and Cu-ferrierite, respectively) and *β*-2 sites (9.6 and 12.0 kcal/mol for Co-ferrierite and Cu-ferrierite, respectively), while the stabilization energy of the *β*-1 site is small (1.4 and 2.1 kcal/mol for Co-ferrierite and Cu-ferrierite, respectively).

6.1.2. NO-Co-Ferrierite and NO-Cu-Ferrierite. Figures 6−8 and Figures S7−S12 depict the optimized structures before and after MD calculations of the three cationic sites of NO-Co-ferrierite and NO-Cu-ferrierite. We will discuss in detail only the geometries after MD.

The Co-O bonds in NO-Co-ferrierite are elongated by up to 0.16 Å (*β*-2) relative to those in Co-ferrierite. Two Co-O bonds remain longer than the others. Conversely, three Cu-O bonds in NO-Cu-ferrierite are slightly elongated by a few hundredths of an angstrom with respect to those in Cu-ferrierite while the remaining fourth Cu-O bond is significantly longer (3.082 (*α*), 2.460 (*β*-1), and 2.697, and 2.836 Å (*β*-2)) than that in Cu-ferrierite (1.89−2.22 Å). During the MD simulations the long Cu-O bond dynamically changes into a short one while one of the short bonds becomes the long one and so forth.

The calculated Co-N bond distances are around 1.68 Å for three cationic sites of NO-Co-ferrierite while the Cu-N bond lengths somewhat differ (1.82−1.88 Å) for the four complexes

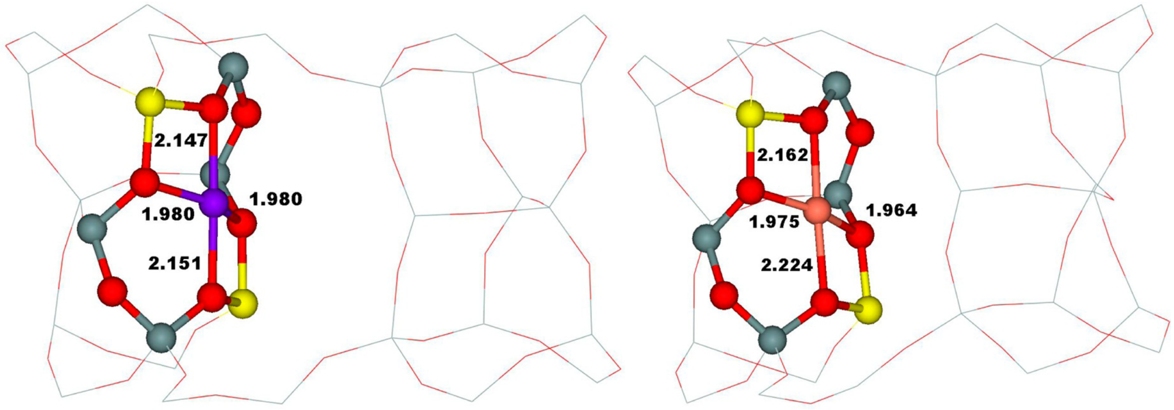

Figure 4. Optimized structures of the α site of Co-ferrierite (left) and Cu-ferrierite (right) after molecular dynamics simulations. The distances are in angstroms. Silicon atoms are in gray, oxygen atoms in red, aluminum atoms in yellow, cobalt atom in violet, and copper atom in pink.

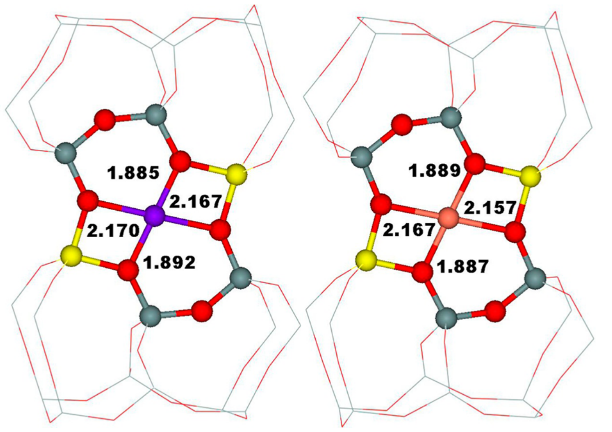

Figure 5. Optimized structures of the β-2 site of Co-ferrierite (left) and Cu-ferrierite (right) after molecular dynamics simulations. The distances are in angstroms. Silicon atoms are in gray, oxygen atoms in red, aluminum atoms in yellow, cobalt atom in violet, and copper atom in pink.

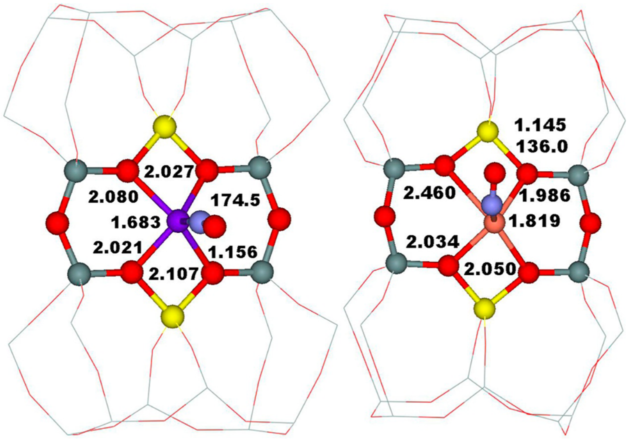

Figure 6. Optimized structures of the β-1 site of NO-Co-ferrierite (left) and NO-Cu-ferrierite (right) after molecular dynamics simulations. The distances are in angstroms and the bond angle in degrees. Silicon atoms are in gray, oxygen atoms in red, aluminum atoms in yellow, nitrogen atom in blue, cobalt atom in violet, and copper atom in pink.

of NO-Cu-ferrierite. It should be noted that the one significant structural difference between the NO-Co-ferrierite and NO-Cu-ferrierite complexes is the Me-N-O angle. The Co-N-O bond angle is around 174° for the α and β-1 sites and 165° for the β-2 site, while the Cu-N-O bond angle is much sharper ranging from 126° (α) to 136° (β-1).

Similar to the case of Co-ferrierite and Cu-ferrierite, MD simulations of NO-Co-ferrierite and NO-Cu-ferrierite resulted into the energy stabilizations (Table 1) with respect to the corresponding structures which were simply optimized without MD. The corresponding energy decrease is significantly smaller than that for the bare Me-ferrierites for the α site (2.5 and 5.6 kcal/mol for Me = Co and Cu, respectively) while it is slightly larger for the β-1 site (1.6 and 3.6 kcal/mol for Me = Co, Cu). The stabilization energy remains the same for NO-Me-ferrierite and Me-ferrierite for the β-2 site (Table 1).

6.2. NO Adsorption Energies.

Table 2 lists the ΔE_{ads} values of NO on Cu-ferrierite and Co-ferrierite. The adsorption is stronger on Co (from −40 to −46 kcal/mol) than on Cu (from −11 to −31 kcal/mol). The ΔE_{ads} values are in the order α (−46 (Co) and −31 (Cu) kcal/mol) > β-2 (−41 (Co) and −20 (Cu) kcal/mol) > β-1 (−40 (Co) and −11 (Cu) kcal/mol) for both cations.

6.3. NO Stretching Frequencies.

The calculated frequencies of the stretching mode of NO adsorbed on Cu and Co cations for the three models optimized before and after MD are shown in Table 3. The former frequencies (before MD) only serve to investigate the effect of the rearrangement of cationic sites while the latter (after MD) are used for a comparison with experiments.

The calculated frequencies (Table 3) are harmonic, and for a comparison with experiments, anharmonic corrections have to be applied. This correction was calculated for the stretching frequency of NO adsorbed on Fe-ferrierite to be 27 cm^{-1}.[35,36] We assume that this correction has a similar value also for NO adsorbed on Co-ferrierite and Cu-ferrierite.

6.4. Relative Binding Energies of Co(II) and Cu(II).

Table 4 shows the $\Delta \mathrm{BE}_{\mathrm{Me}}$ values of Co(II) and Cu(II) in Co-ferrierite and Cu-ferrierite, respectively. Both the cations bind the most tightly in the β-1 site, followed by the β-2 site. The binding is the weakest in the α site.

7. DISCUSSION

In this section, we discuss the changes of the structure and the stabilization energies of the cationic sites upon accommodation of Me(II) cations (section 7.1) and, further, upon formation of complexes of NO with Me(II) (section 7.2). Then, by using

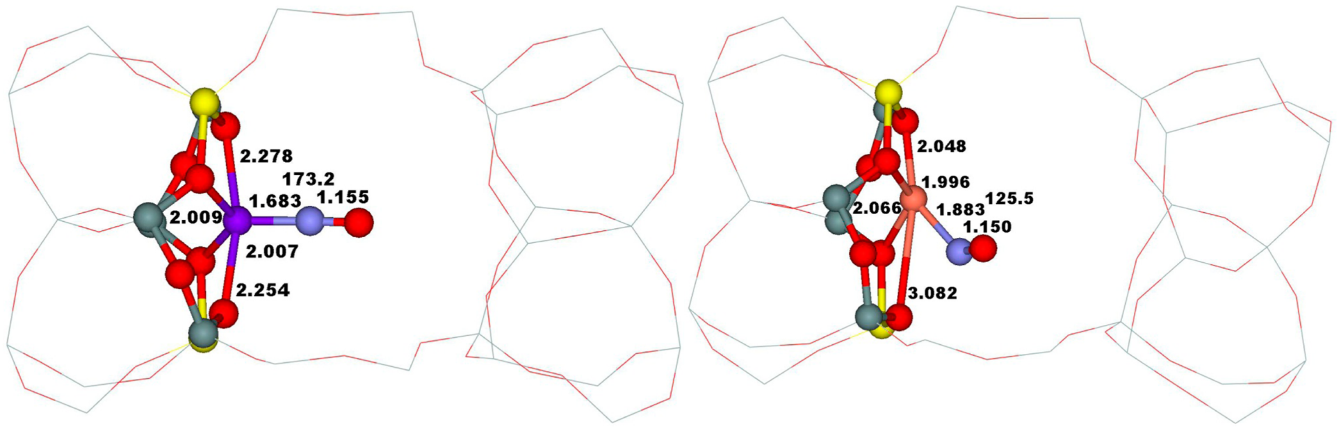

Figure 7. Optimized structures of the α site of NO-Co-ferrierite (left) and NO-Cu-ferrierite (right) after molecular dynamics simulations. The distances are in angstroms and the bond angle in degrees. Silicon atoms are in gray, oxygen atoms in red, aluminum atoms in yellow, nitrogen atom in blue, cobalt atom in violet, and copper atom in pink.

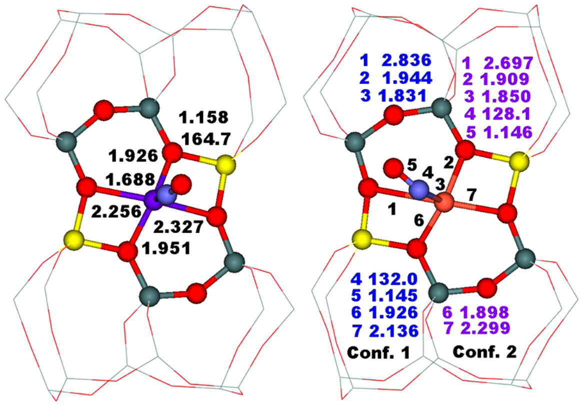

Figure 8. Optimized structures of the β-2 site of NO-Co-ferrierite (left) and NO-Cu-ferrierite (right) after molecular dynamics simulations. The distances are in angstroms and the bond angle in degrees. Silicon atoms are in gray, oxygen atoms in red, aluminum atoms in yellow, nitrogen atom in blue, cobalt atom in violet, and copper atom in pink.

Table 2. Calculated NO Adsorption Energies in kcal/mol of NO-Co-Ferrierite and NO-Cu-Ferrierite Optimized before and after MD

	cationic sites		
	α	β-1	β-2
NO-Co-ferrierite before MD	−49.8	−39.9	−41.0
NO-Co-ferrierite after MD[a]	−46.3	−40.2	−41.1
NO-Cu-ferrierite before MD	−36.5	−9.9	−20.0
NO-Cu-ferrierite after MD[a]	−31.4	−11.4	−20.0

[a]These calculated values can be compared with experiments.

FTIR spectroscopy of metal−cation complexes of ferrierite with a NO molecule, we examine (section 7.3) the possible determination of the types of cationic sites and the Al siting in the six-membered rings forming these cationic sites. Finally, we discuss the ΔBE_{Me} values of Me(II) in cationic sites (section 7.4) and thus their general tendencies to react.

7.1. REARRANGEMENT OF CATIONIC SITES ACCOMMODATING CU AND CO

The structure of sites binding divalent cations were estimated using X-ray diffraction experiments for ferrierite frameworks.[21−24] However, as explained in detail in our prior publication regarding Fe-ferrierite,[25] the obtained structures suffer from a significant decrease in the accuracy of the determined structure of the framework oxygen atoms involved in coordinating the divalent cation. Conversely, the structure of sites accommodating a divalent cation can be inferred from theoretical calculations.[25]

Table 3. Calculated Harmonic[a] and Observed NO Stretching Frequencies in cm^{-1} of NO-Co-Ferrierite and NO-Cu-Ferrierite Optimized before and after MD

	cationic sites		
	α	β-1	β-2
NO-Co-ferrierite before MD	1969	1946	1940
NO-Co-ferrierite after MD[b]	1973	1955	1943
NO-Co-ferrierite observed	1956	1941	1935
NO-Cu-ferrierite before MD	1937	1931	1905
NO-Cu-ferrierite after MD[b]	1897	1940	1931, 1918[c]
NO-Cu-ferrierite observed	1864	1912	1904, 1892

[a]The values are not corrected for anharmonicity. The calculated harmonic frequency of NO(g) is 1906 cm^{-1} while the corresponding experimental value is 1876 cm^{-1}. [b]These calculated values can be compared with experiments. [c]The two values correspond to two distinct conformers.

Table 4. Relative Binding Energies in kcal/mol of Co(II) and Cu(II) in Co-Ferrierite and Cu-Ferrierite, Respectively[a]

	cationic sites		
	α	β-1	β-2
Co-ferrierite before MD	11.9	0.0	13.2
Co-ferrierite after MD[b]	7.2	0.0	5.0
Cu-ferrierite before MD	19.3	0.0	14.8
Cu-ferrierite after MD[b]	10.4	0.0	4.9

[a]The relative energies of the ferrierite with empty cationic sites are as follows: 0.0 for β-1, 7.9 for β-2, and 19.2 for α kcal/mol. [b]These calculated values can be compared with experiments.

Divalent metal cations accommodated in cationic sites have a tendency to coordinate to oxygen atoms of AlO_4^- tetrahedra rather than SiO_4 tetrahedra, since the cations balance the negative charge of AlO_4^-.[25] However, the starting structures feature this proper coordination of Me(II) to four oxygen atoms of two AlO_4^- tetrahedra only for the β-1 site (Figures S1 and S2), while the cations are ligated to only three and two oxygen atoms of two AlO_4^- tetrahedra for the α and β-2 (Figures S3−S6) sites, respectively. The other one (α site) and two (β-2) oxygen atoms belong to SiO_4 tetrahedra. Therefore, the structures of the α and β-2 sites coordinating Me noticeably rearrange during the MD computations. The Me(II) cations properly coordinate to four oxygen atoms of two AlO_4^- tetrahedra in the resulting structures. These results are close to those obtained for Fe-ferrierite.[25] The calculated stabilization energies for Co-ferrierite are smaller than those computed for Cu-ferrierite and Fe-ferrierite which are close to each other (Table 1).

7.2. Structural and Energy Changes after NO Binding.

Essentially the same rearrangement of the cationic sites as for Co-ferrierite is obtained for NO-Co-ferrierite (Figures 6−8). The structures of all the three cationic sites remain very similar to those of Co-ferrierite before NO adsorption. Only the Co-O bonds are elongated relative to those in Co-ferrierite, indicating a weaker coordination of the metal cation to the zeolite framework after the adsorption of NO. Such a decrease of the interaction between the cation and framework of the zeolite due to the interaction with a ligand is well documented experimentally.[46,49,50]

MD simulations of NO-Cu-ferrierite also lead to the structures of the relaxed cationic sites with proper binding of Cu to O atoms of two AlO_4^- tetrahedra, but with one difference. Three Cu-O bonds in NO-Cu-ferrierite are shorter while the remaining fourth Cu-O bond is significantly longer revealing a tendency of Cu(II) with ligated NO to coordinate to only three O atoms of two AlO_4^- tetrahedra rather than to four O (Figures 6−8).

The calculated ΔE_{ads} values (Table 2) indicate a stronger tendency for Co(II) over Cu(II), to form a complex with NO. The strongest adsorption is computed for both the cations accommodated in the α site. According to our computational results, NO coordinates significantly stronger to Cu(II) accommodated in β-2 than β-1, while there is a negligible difference between these two sites for NO adsorbed on Co(II).

7.3. Determination of the Cationic Sites and the Al Siting in the Rings Forming Them.

NO is widely recognized as an effective probe of the local coordination environment of transition metal cations accommodated in zeolite frameworks.[80,81] As shown in this study, FTIR spectroscopy of complexes of NO and Me(II)-exchanged ferrierites can also serve to determine the type of the site in ferrierite and, more importantly, the arrangements of Al-O-Si-O-Si-O-Al in the six-membered rings forming cationic sites.

The agreement between the theoretical NO stretching frequencies calculated employing the rearranged structures of the cationic site accommodating Me(II) and corrected for anharmonicity (see section 6.3,) and the experimental NO stretching frequencies for both Co-ferrierite and Co-ferrierite allows assignment of the observed frequencies to the individual types of cationic sites. For NO-Co-ferrierite, the IR bands found at 1956, 1941, and 1935 cm^{-1} can be assigned to NO-Co complexes with Co(II) located in the α, β-1, and β-2 sites, respectively. Similarly, for NO-Cu-ferrierite, the frequencies of 1864, 1912, 1904, and 1892 cm^{-1} belong to NO-Cu complexes having Cu(II) accommodated in the α, β-1, β-2 (conformer 1), and β-2 (conformer 2) sites, respectively. Two individual IR bands can be assigned to the β-2 site for which two distinct conformers were found. The agreement between the calculated and observed frequencies is significantly better for Cu-ferrierite than for Co-ferrierite, but the assignment is safe for both metal zeolites.

Chakarova and Hadjiivanov[82] suggested a presence of Co(III) species in their Co-ferrierite sample and assigned the IR band at 1934 cm^{-1} to a mononitrosyl complex formed on Co(III). We assume that exclusively Co(II) cations are accommodated in cationic sites in the sample used due to a low Co/Al ratio of our sample and, moreover, a high concentration of framework Al atoms in Al-O-Si-O-Si-O-Al sequences forming cationic sites for divalent cations.[25,44,45] Furthermore, our DFT calculations reveal that the NO stretching frequencies of mononitrosyl complexes formed on Co(II) accommodated in the α, β-1, and β-2 sites are in agreement with the observed frequencies of 1956, 1941, and 1935 cm^{-1}, indicating that these measured frequencies do not belong to a mononitrosyl complex formed on Co(III).

Our results also reveal that the NO stretching frequencies corresponding to the three cationic sites of Cu-ferrierite calculated employing the structures of NO-Me-ferrierite simply optimized using the structure determined by neutron diffraction[66] as the starting geometry (before MD) and the frequencies computed for the rearranged cationic sites (after MD) markedly differ (Table 3). The change is the largest for the α site (1897 cm^{-1} (after MD) vs 1937 cm^{-1} (before MD)). Also, the order of the calculated frequencies changes when the cationic sites rearrange. These results show that using MD simulations, or other similar global optimization techniques which allow the structural rearrangement of cationic sites upon binding divalent cations, are needed to obtain reliable local structures of these cationic sites as well as vibrational frequencies of the probe molecules coordinating to Me(II). The FTIR spectrum of NO-Cu-ferrierite (Figure 2) can be only interpreted using the calculated NO stretching frequencies for the rearranged sites. The band at 1864 cm^{-1}, which was assigned to the α site based on our calculations of the relaxed structures of the cationic sites (after MD), cannot be assigned to any site using the frequencies calculated for the structures which were not relaxed by employing MD simulations (before MD). Therefore, we can conclude that the agreement between the positions of the IR bands of the measured FTIR spectrum of NO-Cu-ferrierite and the corresponding calculated values provides experimental evidence for the rearrangement of cationic sites upon binding a Cu(II) cation.

Conversely, the results of our calculations revealed that the rearrangements of the cationic sites of NO-Co-ferrierite have little effect on the NO stretching frequencies (Table 3). This explains why the assignment of IR bands of NO in a previous study,[37] which used the structures of cationic sites which were not rearranged, is consistent with the present assignment.

The identification of the α, β-1, and β-2 sites in the ferrierite used by employing FTIR spectroscopy of NO-Co-ferrierite and NO-Cu-ferrierite complexes and the DFT calculations is in agreement with the results of the tentative assignment of the Mössbauer parameters to Fe(II) accommodated in the α, β-1, and β-2 sites for the same parent ferrierite.[45] Both these methods reveal the presence of the two nonequivalent Al sitings in the rings forming the β sites in the ferrierite sample used. Conversely, our previous results indicate that most likely ^{27}Al MQ MAS NMR spectroscopy is not sensitive enough to detect sites with a low population in the zeolite framework since the ^{27}Al NMR resonance corresponding to two Al atoms in the rings forming the β-1 site was not found in the ^{27}Al 3Q MAS NMR spectrum of the same parent ferrierite.[44]

We therefore conclude that FTIR spectroscopy of NO-Co-ferrierite and NO-Cu-ferrierite complexes can serve to identify the Al siting in the rings forming the β sites in ferrierites. This method, however, does not allow a determination of the concentration of framework Al atoms forming the individual cationic sites. To answer an obvious question whether this method might extend to other silicon-rich zeolites is beyond the scope of this study.

7.4. Binding of Me(II) in Cationic Sites of Ferrierite.

Table 4 shows that both Co(II) and Cu(II) prefer to accommodate in the β-1 site of ferrierite while the binding in the other two sites is weaker. This tendency of Me(II) to preferably occupy the β-1 site of ferrierite at a low Me(II)/Al ratio was also found in our Mössbauer spectroscopy study of ^{57}Fe-ferrierite.[45,58] Since the structures of both β-2 and α sites significantly rearrange upon binding the cation, the difference in the ΔBE_{Me} values are smaller, only up to 7 kcal/mol for Co(II) and 10 kcal/mol for Cu(II). When Me-ferrierite is treated at elevated temperature, then the concentration of Me(II) occupying the α site should drop and that of β-2 and especially of β-1 should increase. This effect, i.e., a migration of Me(II) from the α site to the β sites upon thermal treatment, was observed in our prior study of Co-ferrierite.[46]

The general tendency of Me(II) accommodated in a cationic site to react is inversely proportional to the corresponding BE_{Me} values, and therefore it is the highest when Me(II) is accommodated in the α site, as it is the least stabilized. Conversely, Me(II) is the most stabilized in the β-1 site, and therefore, its general tendency to react is the lowest. This trend correlates with the ΔE_{ads} values (Table 2) which are the largest for the α site and the smallest for the β-1 site. However, other factors also significantly influence the reactivity of Me(II) for a particular reaction. Therefore, for individual reactions, the catalytic activity of Me(II) located in the distinct sites does not have to follow the general tendencies of Me(II) to react.

8. CONCLUSIONS

We investigated, employing periodic DFT molecular dynamics and FTIR spectroscopy, the cationic sites of Co-ferrierite and Cu-ferrierite as well as their complexes with NO (NO-Co-ferrierite and NO-Cu-ferrierite). Our calculations show that both the cations upon binding to cationic sites induce a rearrangement of the local structure of the zeolite framework. The principal reason is the tendency for a formation of a structure with metal cation coordination to oxygen atoms of AlO_4^- tetrahedra rather than of SiO_4 tetrahedra. The structural rearrangements as well as stabilization energies are significant for the α (6 (Co) and 11 (Cu) kcal/mol) and β-2 (10 (Co) and 12 (Cu) kcal/mol) sites, while they are small for the β-1 site (1 (Co) and 2 (Cu) kcal/mol).

FTIR spectroscopy of metal−cation complexes with a NO molecule was used to study the local coordination environment of the Me(II) cations located in the active sites and to validate the calculated results. Our calculations allow assignments of the experimental IR bands to the NO-Me-ferrierite complexes: 1956, 1941, and 1935 cm^{-1} to NO-Co located in the α, β-1, and β-2 sites, respectively; 1864, 1912, 1904, and 1892 cm^{-1} to NO-Cu accommodated in the α, β-1, β-2 (conformer 1), and β-2 (conformer 2) sites, respectively. The presence of the band at 1864 cm^{-1} provides experimental evidence for the structural rearrangement of cationic sites since this IR band cannot be assigned to any site using the frequencies calculated for the structures which were not relaxed by employing MD simulations (before MD). Our calculations show that the Al siting in the rings affects the local structure of the zeolite framework upon binding Me(II) as well as the ΔBE_{Me} values. The binding of Me(II) is the strongest in β-1, weaker in β-2, and the weakest in α. Therefore, the general tendency of Me(II) accommodated in cationic sites to react is $\alpha > \beta\text{-}2 > \beta\text{-}1$ as it is inversely proportional to the corresponding ΔBE_{Me} values. These results clearly demonstrate the effects of the Al siting in the rings on the potential catalytic activity of the coordinated Me(II) cations and therefore justify the importance of the knowledge of the Al siting in the rings for understanding the catalytic properties of the Me(II)-exchanged zeolites. Our results further reveal that FTIR spectroscopy of complexes of NO and Me(II)-exchanged ferrierite can serve to identify the Al siting in the six-membered rings forming the β sites.

■ ASSOCIATED CONTENT

Ⓢ Supporting Information

Optimized structures of Co-ferrierite, NO-Co-ferrierite, Cu-ferrierite, and NO-Cu-ferrierite (Figures S1−S12). This material is available free of charge via the Internet at http://pubs.acs.org.

■ AUTHOR INFORMATION

Corresponding Author

*E-mail stepan.sklenak@jh-inst.cas.cz.

Notes

The authors declare no competing financial interest.

■ ACKNOWLEDGMENTS

This study was performed with institutional support RVO:61388955 and further was supported by the Grant Agency of the Academy of Sciences of the Czech Republic (Projects # IAA400400812) and Grant Agency of the Czech Republic (Projects # GA 203/09/1627).

■ REFERENCES

(1) Traa, Y.; Burger, B.; Weitkamp, J. Zeolite-Based Materials for the Selective Catalytic Reduction of NO_x with Hydrocarbons. *Microporous Mesoporous Mater.* **1999**, *30*, 3−41.

(2) Wichtelova, B.; Sobalik, Z.; Dedecek, J. Redox Catalysis over Metallo-Zeolites - Contribution to Environmental Catalysis. *Appl. Catal., B* **2003**, *41*, 97−114.

(3) Forzatti, P.; Nova, I.; Tronconi, E. Enhanced NH_3 Selective Catalytic Reduction for NO_X Abatement. *Angew. Chem., Int. Ed.* **2009**, *48*, 8366−8368.

(4) Shelef, M. Selective Catalytic Reduction of NO_x with N-Free Reductants. *Chem. Rev.* **1995**, *95*, 209−225.

(5) Yahiro, H.; Iwamoto, M. Copper Ion-Exchanged Zeolite Catalysts in deNO_x Reaction. *Appl. Catal., A* **2001**, *222*, 163−181.

(6) Panov, G. I.; Kharitonov, A. S.; Sobolev, V. I. Oxidative Hydroxylation Using Dinitrogen Monoxide - a Possible Route for Organic-Synthesis over Zeolites. *Appl. Catal., A* **1993**, *98*, 1−20.

(7) Perez-Ramirez, J.; Groen, J. C.; Bruckner, A.; Kumar, M. S.; Bentrup, U.; Debbagh, M. N.; Villaescusa, L. A. Evolution of Isomorphously Substituted Iron Zeolites During Activation: Comparison of Fe-beta and Fe-ZSM-5. *J. Catal.* **2005**, *232*, 318−334.

(8) Jisa, K.; Novakova, J.; Schwarze, M.; Vondrova, A.; Sklenak, S.; Sobalik, Z. Role of the Fe-zeolite Structure and Iron State in the N_2O Decomposition: Comparison of Fe-FER, Fe-BEA, and Fe-MFI Catalysts. *J. Catal.* **2009**, *262*, 27−34.

(9) Centi, G.; Perathoner, S. Nature of Active Species in Copper-Based Catalysts and their Chemistry of Transformation of Nitrogen-Oxides. *Appl. Catal., A* **1995**, *132*, 179−259.

(10) Desai, A. J.; Kovalchuk, V. I.; Lombardo, E. A.; d'Itri, J. L. CoZSM-5: Why this Catalyst Selectively Reduces NO_x with Methane. *J. Catal.* **1999**, *184*, 396−405.

(11) Boix, A.; Miro, E. E.; Lombardo, E. A.; Banares, M. A.; Mariscal, R.; Fierro, J. L. G. The Nature of Cobalt Species in Co and PtCoZSM5 Used for the SCR of NO_x with CH_4. *J. Catal.* **2003**, *217*, 186−194.

(12) Resini, C.; Montanari, T.; Nappi, L.; Bagnasco, G.; Turco, M.; Busca, G.; Bregani, F.; Notaro, M.; Rocchini, G. Selective Catalytic Reduction of NO_x by Methane over Co-H-MFI and Co-H-FER Zeolite Catalysts: Characterisation and Catalytic Activity. *J. Catal.* **2003**, *214*, 179−190.

(13) Chen, X. Y.; Shen, S. C.; Chen, H. H.; Kawi, S. SCR of Lean NO_x with C_3H_8 over Co/MFI Catalysts: Dependence on Synthesis Condition of MFI and Co Location. *J. Catal.* **2004**, *221*, 137−147.

(14) Smeets, P. J.; Meng, Q. G.; Corthals, S.; Leeman, H.; Schoonheydt, R. A. Co-ZSM-5 Catalysts in the Decomposition of N_2O and the SCR of NO with CH_4: Influence of Preparation Method and Cobalt Loading. *Appl. Catal., B* **2008**, *84*, 505−513.

(15) Chen, X. M.; Zhu, A. M.; Au, C. T.; Yang, X. F.; Shi, C. A. The Role of Active Sites of CoH-ZSM-5 Catalysts for the C_2H_4-SCR of NO. *Catal. Lett.* **2010**, *135*, 182−189.

(16) Beznis, N. V.; van Laak, A. N. C.; Weckhuysen, B. M.; Bitter, J. H. Oxidation of Methane to Methanol and Formaldehyde over Co-ZSM-5 Molecular Sieves: Tuning the Reactivity and Selectivity by Alkaline and Acid Treatments of the Zeolite ZSM-5 Agglomerates. *Microporous Mesoporous Mater.* **2011**, *138*, 176−183.

(17) Shichi, A.; Satsuma, A.; Hattori, T. Promoting Effect of Water Vapor on the Catalytic Activity of Cobalt-Exchanged MFI Zeolite for the Selective Reduction of NO by C_3H_8. *Chem. Lett.* **2001**, 44−45.

(18) Mortier, W. J. Temperature-Dependent Cation Distribution in Dehydrated Calcium-Exchanged Mordenite. *J. Phys. Chem.* **1977**, *81*, 1334−1338.

(19) Schlenker, J. L.; Pluth, J. J.; Smith, J. V. Positions of Cations and Molecules in Zeolites with Mordenite-Type Framework VI Dehydrated Barium Mordenite. *Mater. Res. Bull.* **1978**, *13*, 169−174.

(20) Mortier, W. J.; Pluth, J. J.; Smith, J. V. Positions of Cations and Molecules in Zeolites with Mordenite-Type Framework I Dehydrated Ca-Exchanged Ptilolite. *Mater. Res. Bull.* **1975**, *10*, 1037−1045.

(21) Dalconi, M. C.; Alberti, A.; Cruciani, G. Cation Migration and Structural Modification of Co-Exchanged Ferrierite upon Heating: A Time-Resolved X-Ray Powder Diffraction Study. *J. Phys. Chem. B* **2003**, *107*, 12973−12980.

(22) Dalconi, M. C.; Alberti, A.; Cruciani, G.; Ciambelli, P.; Fonda, E. Siting and Coordination of Cobalt in Ferrierite: XRD and EXAFS Studies at Different Co Loadings. *Microporous Mesoporous Mater.* **2003**, *62*, 191−200.

(23) Dalconi, M. C.; Cruciani, G.; Alberti, A.; Ciambelli, P.; Rapacciuolo, M. T. Ni^{2+} Ion Sites in Hydrated and Dehydrated Forms of Ni-Exchanged Zeolite Ferrierite. *Microporous Mesoporous Mater.* **2000**, *39*, 423−430.

(24) Dalconi, M. C.; Cruciani, G.; Alberti, A.; Ciambelli, P. Co- and Ni-Exchanged Ferrierite: The Contribution of Synchrotron X-Ray Diffraction Data to Siting of TMIs. *Catal. Today* **2005**, 345−350.

(25) Sklenak, S.; Andrikopoulos, P. C.; Boekfa, B.; Jansang, B.; Novakova, J.; Benco, L.; Bucko, T.; Hafner, J.; Dedecek, J.; Sobalik, Z. N_2O Decomposition over Fe-zeolites: Structure of the Active Sites and the Origin of the Distinct Reactivity of Fe-ferrierite, Fe-ZSM-5, and Fe-beta. A Combined Periodic DFT and Multispectral Study. *J. Catal.* **2010**, *272*, 262−274.

(26) Hafner, J.; Benco, L.; Bucko, T. Acid-Based Catalysis in Zeolites Investigated by Density-Functional Methods. *Top. Catal.* **2006**, *37*, 41−54.

(27) McMillan, S. A.; Broadbelt, L. J.; Snurr, R. Q. Effect of Local Framework Heterogeneity on NO Adsorption in Cobalt-Ferrierite. *J. Catal.* **2003**, *219*, 117−125.

(28) McMillan, S. A.; Snurr, R. Q.; Broadbelt, L. J. Origin and Characteristics of Preferential Adsorption on Different Sites in Cobalt-Exchanged Ferrierite. *J. Phys. Chem. B* **2003**, *107*, 13329−13335.

(29) Groothaert, M. H.; Pierloot, K.; Delabie, A.; Schoonheydt, R. A. Identification of Cu(II) Coordination Structures in Cu-ZSM-5, Based on a DFT/Ab Initio Assignment of the EPR Spectra. *Phys. Chem. Chem. Phys.* **2003**, *5*, 2135−2144.

(30) Banach, E.; Kozyra, P.; Rejmak, P.; Broclawik, E.; Datka, J. Cobalt Cationic Sites in Ferrierites: QM/MM Modeling. *Catal. Today* **2008**, *137*, 493−497.

(31) Li, G. N.; Pidko, E. A.; van Santen, R. A.; Feng, Z. C.; Li, C.; Hensen, E. J. M. Stability and Reactivity of Active Sites for Direct Benzene Oxidation to Phenol in Fe/ZSM-5: A Comprehensive Periodic DFT Study. *J. Catal.* **2011**, *284*, 194−206.

(32) Benco, L.; Bucko, T.; Hafner, J. Dehydrogenation of Propane over Zn-MOR. Static and Dynamic Reaction Energy Diagram. *J. Catal.* **2011**, *277*, 104−116.

(33) Goltl, F.; Hafner, J. Structure and Properties of Metal-Exchanged Zeolites Studied Using Gradient-Corrected and Hybrid Functionals. I. Structure and Energetics. *J. Chem. Phys.* **2012**, *136*, 064501.

(34) Goltl, F.; Hafner, J. Structure and Properties of Metal-Exchanged Zeolites Studied Using Gradient-Corrected and Hybrid Functionals. II. Electronic Structure and Photoluminescence Spectra. *J. Chem. Phys.* **2012**, *136*, 064502.

(35) Benco, L.; Bucko, T.; Grybos, R.; Hafner, J.; Sobalik, Z.; Dedecek, J.; Hrusak, J. Adsorption of NO in Fe^{2+}-Exchanged Ferrierite. A Density Functional Theory Study. *J. Phys. Chem. C* **2007**, *111*, 586−595.

(36) Benco, L.; Bucko, T.; Grybos, R.; Hafner, J.; Sobalik, Z.; Dedecek, J.; Sklenak, S.; Hrusak, J. Multiple Adsorption of NO on Fe^{2+} Cations in the α- and β-Positions of Ferrierite: An Experimental and Density Functional Study. *J. Phys. Chem. C* **2007**, *111*, 9393−9402.

(37) Georgieva, I.; Benco, L.; Tunega, D.; Trendafilova, N.; Hafner, J.; Lischka, H. Multiple Adsorption of NO on Cobalt-Exchanged Chabazite, Mordenite, and Ferrierite Zeolites: A Periodic Density Functional Theory Study. *J. Chem. Phys.* **2009**, *131*, 054101.

(38) Grybos, R.; Hafner, J.; Benco, L.; Raybaud, P. Adsorption of NO on Pd-Exchanged Mordenite: Ab Initio DFT Modeling. *J. Phys. Chem. C* **2008**, *112*, 12349−12362.

(39) Goltl, F.; Hafner, J. Structure and Properties of Metal-Exchanged Zeolites Studied Using Gradient-Corrected and Hybrid Functionals. III. Energetics and Vibrational Spectroscopy of Adsorbates. *J. Chem. Phys.* **2012**, *136*, 064503.

(40) Eight-membered ring in the case of the β site of mordenite.

(41) Takaishi, T.; Kato, M.; Itabashi, K. Stability of the Al-O-Si-O-Al Linkage in a Zeolitic Framework. *J. Phys. Chem.* **1994**, *98*, 5742−5743.

(42) Takaishi, T.; Kato, M.; Itabashi, K. Determination of the Ordered Distribution of Aluminum Atoms in a Zeolitic Framework. Part II. *Zeolites* **1995**, *15*, 21−32.

(43) Fe(II) accommodated in the β-1 site is less reactive than that located in the β-2 site. N_2O does not adsorb via the O atom on Fe(II) accommodated in isolated β-1 sites.

(44) Dedecek, J.; Lucero, M. J.; Li, C. B.; Gao, F.; Klein, P.; Urbanova, M.; Tvaruzkova, Z.; Sazama, P.; Sklenak, S. Complex Analysis of the Aluminum Siting in the Framework of Silicon-Rich Zeolites. A Case Study on Ferrierites. *J. Phys. Chem. C* **2011**, *115*, 11056−11064.

(45) Tabor, E.; Zaveta, K.; Sathu, N. K.; Tvaruzkova, Z.; Sobalik, Z. Characterization of Iron Cationic Sites in Ferrierite Using Mössbauer Spectroscopy. *Catal. Today* **2011**, *169*, 16−23.

(46) Sobalik, Z.; Dedecek, J.; Kaucky, D.; Wichterlova, B.; Drozdova, L.; Prins, R. Structure, Distribution, and Properties of Co Ions in Ferrierite Revealed by FTIR, UV-Vis, and EXAFS. *J. Catal.* **2000**, *194*, 330−342.

(47) Dedecek, J.; Capek, L.; Sazama, P.; Sobalik, Z.; Wichterlova, B. Control of Metal Ion Species in Zeolites by Distribution of Aluminium in the Framework: From Structural Analysis to Performance under Real Conditions of SCR-NO*x* and NO, N_2O Decomposition. *Appl. Catal., A* **2011**, *391*, 244−253.

(48) Kaucky, D.; Dedecek, J. I.; Wichterlova, B. Co^{2+} Ion Siting in Pentasil-Containing Zeolites: II. Co^{2+} Ion Sites and their Occupation

in Ferrierite. A VIS Diffuse Reflectance Spectroscopy Study. *Microporous Mesoporous Mater.* **1999**, *31*, 75−87.

(49) Sobalik, Z.; Tvaruzkova, Z.; Wichterlova, B. Skeletal T-O-T Vibrations as a Tool for Characterization of Divalent Cation Complexation in Ferrierite. *J. Phys. Chem. B* **1998**, *102*, 1077−1085.

(50) Dedecek, J.; Sobalik, Z.; Wichterlova, B. Siting and Distribution of Framework Aluminium Atoms in Silicon-Rich Zeolites and Impact on Catalysis. *Catal. Rev.* **2012**, *54*, 135−223.

(51) Boronat, M.; Martinez-Sanchez, C.; Law, D.; Corma, A. Enzyme-Like Specificity in Zeolites: A Unique Site Position in Mordenite for Selective Carbonylation of Methanol and Dimethyl Ether with CO. *J. Am. Chem. Soc.* **2008**, *130*, 16316−16323.

(52) Boronat, M.; Martinez, C.; Corma, A. Mechanistic Differences between Methanol and Dimethyl Ether Carbonylation in Side Pockets and Large Channels of Mordenite. *Phys. Chem. Chem. Phys.* **2011**, *13*, 2603−2612.

(53) Capek, L.; Dedecek, J.; Wichterlova, B. Co-beta Zeolite Highly Active in Propane-SCR-NO_x in the Presence of Water Vapor: Effect of Zeolite Preparation and Al Distribution in the Framework. *J. Catal.* **2004**, *227*, 352−366.

(54) Capek, L.; Dedecek, J.; Wichterlova, B.; Cider, L.; Jobson, E.; Tokarova, V. Cu-ZSM-5 Zeolite Highly Active in Reduction of NO with Decane - Effect of Zeolite Structural Parameters on the Catalyst Performance. *Appl. Catal., B* **2005**, *60*, 147−153.

(55) Dedecek, J.; Capek, L.; Wichterlova, B. Nature of Active Sites in Decane-SCR-NO_x and NO Decomposition over Cu-ZSM-5 Zeolites. *Appl. Catal., A* **2006**, *307*, 156−164.

(56) Sazama, P.; Dedecek, J.; Gabova, V.; Wichterlova, B.; Spoto, G.; Bordiga, S. Effect of Aluminium Distribution in the Framework of ZSM-5 on Hydrocarbon Transformation. Cracking of 1-Butene. *J. Catal.* **2008**, *254*, 180−189.

(57) Capek, L.; Dedecek, J.; Sazama, P.; Wichterlova, B. The Decisive Role of the Distribution of Al in the Framework of Beta Zeolites on the Structure and Activity of Co Ion Species in Propane-SCR-NO_x in the Presence of Water Vapour. *J. Catal.* **2010**, *272*, 44−54.

(58) Tabor, E.; Zaveta, K.; Sathu, N. K.; Vondrova, A.; Sazama, P.; Sobalik, Z. N_2O Decomposition over Fe-FER: A Mössbauer Study of the Active Sites. *Catal. Today* **2011**, *175*, 238−244.

(59) Sklenak, S.; Dedecek, J.; Li, C. B.; Wichterlova, B.; Gabova, V.; Sierka, M.; Sauer, J. Aluminum Siting in Silicon-Rich Zeolite Frameworks: A Combined High-Resolution ^{27}Al NMR Spectroscopy and Quantum Mechanics/Molecular Mechanics Study of ZSM-5. *Angew. Chem., Int. Ed.* **2007**, *46*, 7286−7289.

(60) van Bokhoven, J. A.; Lee, T. L.; Drakopoulos, M.; Lamberti, C.; Thiess, S.; Zegenhagen, J. Determining the Aluminium Occupancy on the Active T-Sites in Zeolites Using X-Ray Standing Waves. *Nat. Mater.* **2008**, *7*, 551−555.

(61) Sklenak, S.; Dedecek, J.; Li, C.; Wichterlova, B.; Gabova, V.; Sierka, M.; Sauer, J. Aluminium Siting in the ZSM-5 Framework by Combination of High Resolution ^{27}Al NMR and DFT/MM Calculations. *Phys. Chem. Chem. Phys.* **2009**, *11*, 1237−1247.

(62) Dedecek, J.; Sklenak, S.; Li, C.; Wichterlova, B.; Gabova, V.; Brus, J.; Sierka, M.; Sauer, J. Effect of Al-Si-Al and Al-Si-Si-Al Pairs in the ZSM-5 Zeolite Framework on the ^{27}Al NMR Spectra. A Combined High-Resolution ^{27}Al NMR and DFT/MM Study. *J. Phys. Chem. C* **2009**, *113*, 1447−1458.

(63) Dedecek, J.; Sklenak, S.; Li, C. B.; Gao, F.; Brus, J.; Zhu, Q. J.; Tatsumi, T. Effect of Al/Si Substitutions and Silanol Nests on the Local Geometry of Si and Al Framework Sites in Silicone-Rich Zeolites: A Combined High Resolution ^{27}Al and ^{29}Si NMR and Density Functional Theory/Molecular Mechanics Study. *J. Phys. Chem. C* **2009**, *113*, 14454−14466.

(64) Dedecek, J.; Kaucky, D.; Wichterlova, B. Al Distribution in ZSM-5 Zeolites: An Experimental Study. *Chem. Commun.* **2001**, 970−971.

(65) Dedecek, J.; Kaucky, D.; Wichterlova, B.; Gonsiorova, O. Co^{2+} Ions as Probes of Al Distribution in the Framework of Zeolites. ZSM-5 Study. *Phys. Chem. Chem. Phys.* **2002**, *4*, 5406−5413.

(66) Pickering, I. J.; Maddox, P. J.; Thomas, J. M.; Cheetham, A. K. A Neutron Powder Diffraction Analysis of Potassium-Exchanged Ferrierite. *J. Catal.* **1989**, *119*, 261−265.

(67) Kresse, G.; Furthmuller, J. Efficient Iterative Schemes for *Ab Initio* Total-Energy Calculations Using a Plane-Wave Basis Set. *Phys. Rev. B* **1996**, *54*, 11169−11186.

(68) Kresse, G.; Furthmuller, J. Efficiency of Ab-Initio Total Energy Calculations for Metals and Semiconductors Using a Plane-Wave Basis Set. *Comput. Mater. Sci.* **1996**, *6*, 15−50.

(69) Kresse, G.; Hafner, J. *Ab Initio* Molecular-Dynamics for Open-Shell Transition-Metals. *Phys. Rev. B* **1993**, *48*, 13115−13118.

(70) Kresse, G.; Hafner, J. *Ab Initio* Molecular-Dynamics Simulation of the Liquid-Metal-Amorphous-Semiconductor Transition in Germanium. *Phys. Rev. B* **1994**, *49*, 14251−14269.

(71) Blöchl, P. E. Projector Augmented-Wave Method. *Phys. Rev. B* **1994**, *50*, 17953−17979.

(72) Kresse, G.; Joubert, D. From Ultrasoft Pseudopotentials to the Projector Augmented-Wave Method. *Phys. Rev. B* **1999**, *59*, 1758−1775.

(73) Perdew, J. P.; Chevary, J. A.; Vosko, S. H.; Jackson, K. A.; Pederson, M. R.; Singh, D. J.; Fiolhais, C. Atoms, Molecules, Solids, and Surfaces: Applications of the Generalized Gradient Approximation for Exchange and Correlation. *Phys. Rev. B* **1992**, *46*, 6671−6687.

(74) Perdew, J. P.; Wang, Y. Accurate and Simple Analytic Representation of the Electron-Gas Correlation-Energy. *Phys. Rev. B* **1992**, *45*, 13244−13249.

(75) Nose, S. A. Unified Formulation of the Constant Temperature Molecular-Dynamics Methods. *J. Chem. Phys.* **1984**, *81*, 511−519.

(76) Verlet, L. Computer "Experiments" on Classical Fluids. I. Thermodynamical Properties of Lennard-Jones Molecules. *Phys. Rev.* **1967**, *159*, 98−103.

(77) Verlet, L. Computer "Experiments" on Classical Fluids. II. Equilibrium Correlation Functions. *Phys. Rev.* **1968**, *165*, 201−214.

(78) Kresse, G.; Furthmuller, J.; Hafner, J. *Ab Initio* Force Constant Approach to Phonon Dispersion Relations of Diamond and Graphite. *Europhys. Lett.* **1995**, *32*, 729−734.

(79) McMillan, S. A.; Snurr, R. Q.; Broadbelt, L. J. Interaction of Divalent Metal Cations with Ferrierite: Insights from Density Functional Theory. *Microporous Mesoporous Mater.* **2004**, *68*, 45−53.

(80) Lamberti, C.; Zecchina, A.; Groppo, E.; Bordiga, S. Probing the Surfaces of Heterogeneous Catalysts by *In Situ* IR Spectroscopy. *Chem. Soc. Rev.* **2010**, *39*, 4951−5001.

(81) Hadjiivanov, K. I. Identification of Neutral and Charged N_xO_y Surface Species by IR Spectroscopy. *Catal. Rev.* **2000**, *42*, 71−144.

(82) Chakarova, K.; Hadjiivanov, K. Coordination Chemistry of Cobalt Ions in Ferrierite: An FTIR Spectroscopic Study. *Microporous Mesoporous Mater.* **2009**, *123*, 123−128.